Hindawi
Advances in Civil Engineering
Volume 2020, Article ID 2765193, 16 pages
https://doi.org/10.1155/2020/2765193

Research Article

Out-of-Plane Bending and Shear Behaviors of Steel Plate-Concrete Walls for Nuclear Power Plants

Zhihua Chen,[1,2] Jingshu Wu ,[1,3] Jiadi Liu,[1] and Chenghe Hu[3]

[1]*Department of Civil Engineering, Tianjin University, Tianjin, 300354, China*
[2]*State Key Laboratory of Hydraulic Engineering Simulation and Safety, Tianjin, 300354, China*
[3]*Research Institute of Building and Construction Co. Ltd. MCC Group, Beijing, 100088, China*

Correspondence should be addressed to Jingshu Wu; suesue.wu@126.com

Received 26 September 2019; Revised 18 March 2020; Accepted 20 April 2020; Published 11 May 2020

Academic Editor: José Aguiar

The steel plate-concrete structure, with its advantages of modular construction, good seismic capacity, and strong impact resistance, has been gradually replacing the reinforced concrete structure in the containment vessel and internal workshop structure of nuclear power plants in recent years. In this study, the out-of-plane single-point loading test and parametric finite element simulation analysis were conducted on five steel plate-concrete wall slab specimens with different stud spacings, shear span ratios, and steel contents. Results showed that the steel plate-concrete wall slab under the out-of-plane load had the same failure mode as that of an ordinary reinforced concrete wall. The out-of-plane shear capacity of the steel plate-concrete wall slab increased significantly in the case of numerous studs. With the increase in shear span ratio, steel plate-concrete members suffered a bending failure. When the steel content was low, they had diagonal tension failure, such as a rare-reinforced concrete wall. The out-of-plane bending and shear mechanism of the steel plate-concrete shear wall was studied theoretically, and the calculation formulas of the bending and shearing capacities were derived.

1. Introduction

The characteristics of the steel plate-concrete structure are high bearing capacity, good ductility, excellent seismic performance, and impact resistance. This new type of structure enables modular construction and installation. Therefore, the steel plate-concrete structure has been intensively applied in engineering, specifically in many important infrastructures and key projects.

In recent years, a series of studies on the steel plate-concrete structure has been conducted locally and internationally. Masayuki Takeuchi et al. tested steel plate-concrete members, via single-point, two-point, and antisymmetrical loadings; they analyzed the influence of shear span ratio on the cracking load and ultimate bearing capacity of the members [3]. Okutani investigated the out-of-plane behavior of steel plate-concrete members and found that shear span ratio and stud spacing exert remarkable effects on the performance of members [4, 5]. Tetsuya Toyoda et al. calculated the crack strength of steel plate-concrete structural members by using the theoretical deduction method [6]. Ikeda et al. deduced the out-of-plane shear calculation model and bearing capacity calculation formula suitable for the truss-arch coupon structure of the steel plate-concrete structure through theoretical research [7]. Yoichi proposed a formula to calculate the out-of-plane bearing capacity of unilateral steel plate-concrete members [8]. Hong et al. discussed the influence of the bond strength of studs on the strength of diagonal struts in the arch load-bearing mechanism on the basis of the Japanese JEAC-4618-2009 regulation; they deduced the corresponding mechanical calculation model [9]. In 2011, Varma et al. (American scholars) conducted out-of-plane shear tests on two groups of steel plate-concrete beam specimens with and without stiffeners; they studied the shear span ratio, steel plate thickness, shear reinforcement ratio, and other related parameters. The results showed that the out-of-plane shear capacity of the steel sheet concrete wall is provided by the shear resistance of the shear reinforcement and concrete [10].

At present, domestic scholars have conducted relevant research on the out-of-plane performance of steel plate-concrete members. Liu Zongxian and Cao Zhiyuan from the Institute of Mechanics, Chinese Academy of Sciences, provided the basic dynamic equation and equivalent combined coefficients of the elasticity of plates by using the equivalent nonclassical theory of composite plates; they obtained the analytic solutions of the natural frequency and dynamic response of plate structures on steel plate coagulation [11]. Nie Jianguo et al. conducted antisymmetrical loading tests on eight simply supported steel plate-concrete beams; they concluded that the rational layout of studs plays a key role in the steel plate-concrete members. After the theoretical analysis of the cracking load of the steel plate-concrete structure, they obtained the elastic theory calculation formula [12]. Yang Fang and Sun Yunlun confirmed that the calculation method of the out-of-plane bearing capacity of concrete-filled rectangular steel tubular members can be used to evaluate the bearing capacity of steel plate-concrete members through theoretical calculation [14]. Leng Yubing et al. investigated the beam specimens with the built-in shear channel steel and steel plate-concrete-steel plate Sandwich slab structure; they deduced the theoretical model for calculating the out-of-plane bearing capacity of the abovementioned Sandwich slab structure under a concentrated load based on experiments [15–17]. Yang Yue et al. analyzed the influencing degrees of steel plate thickness, steel bar configuration, and shear connector through bending tests on unilateral and bilateral steel plate-concrete slabs [18]. Ji Xiaodong et al. performed quasi-static tests on concrete wall specimens embedded and encased with a steel plate under a reciprocating shear and constant axial pressure to analyze the shear behavior of the steel plate-concrete shear wall comprehensively [19]. Chen Chao and Song Xiaobing from Shanghai Jiaotong University established an internal biaxial tension-compression cyclic loading model, which comprises the planes of steel plate-concrete component elements [20].

A series of studies have been conducted locally and internationally on steel plate-concrete walls in ordinary high-rise buildings in recent years. However, the existing theory cannot be directly applied due to the significant difference between the nuclear power plants and ordinary high-rise buildings in terms of the material and structure of steel plate-concrete members, which present different mechanical properties and structural stress states. Therefore, the steel plate-concrete members used in nuclear power plants in the field of nuclear power safety must be investigated. In this study, a series of experiments were conducted on the out-of-plane behaviors of the steel-concrete composite shear wall on the basis of the structural form of the CAP1400 steel-concrete composite shear wall. The aim is to analyze the influences of shear span ratio, section height, and stud spacing on the out-of-plane mechanical properties of the steel-concrete composite shear wall under a large span (shear span ratio > 2.0).

2. Experimental Investigation

Specimens were designed and tested under three-point loading to study the out-of-plane behavior of steel-concrete composite shear walls. The details of the tests are discussed in the following sections.

2.1. Details of Specimens. The steel-concrete composite shear wall investigated in this study was composed of steel plates on both sides, concrete filling between steel plates, studs, and truss shear components, as shown in Figure 1. Five groups of specimens were designed in accordance with the requirements on steel plate-concrete members in the Technical Specification for Seismic Design of Steel Plate Concrete Structures (JEAC 4618–2009), numbering SC-P1 to SC-P5. The objective is to explore the influences of stud spacing, shear span ratio, and reinforcement ratio on the out-of-plane mechanical properties of the steel-concrete shear wall structure in the shield workshop of the nuclear power plant. Table 1 shows the parameters of the specimens. The width of the five test specimens is 600 mm, the height of SC-P1–SC-P4 is 450 mm, and the height of SC-P5 is 675 mm. The length of each test specimen varies from 3,100 mm to 7,200 mm. Comparisons were performed between SC-P1 and SC-P2, SC-P3 and SC-P4, and SC-P4 and SC-P5 to analyze the influences of stud spacing, shear span ratio, and steel ratio on the out-of-plane shear capacity of specimens. The Technical Specification for Seismic Design of Steel Plate Concrete Structures (JEAC 4618–2009) provides design procedures for steel plate-concrete members. The composite plate beams can be used to study the performance of the steel-concrete composite shear wall in the experiment.

The Q235B carbon steel was used as the steel plate in the test. The yield strength, ultimate tensile strength, elastic modulus, and steel elongation were determined in accordance with Metallic Materials, Tensile Testing at Ambient Temperature (GB/T 228–2002). Table 2 shows the results. The C30 concrete was adopted. Concrete blocks were reserved when pouring specimens and maintained in the same indoor environment as specimens. The material properties were tested in accordance with the Standard for Test Method of Mechanical Properties on Ordinary Concrete (GB/T50081-2002). Table 3 shows the test results.

2.2. Support and Loading Conditions. The test was performed on a 100-t fatigue testing machine with two-point simple support and single-point loading. The two ends of the specimens are simply supported. The test span of SC-P1–SC-P5 is from 1,800 mm to 4,500 mm, and Table 1 shows the span parameters. Figure 2 depicts the test device. The loading process was controlled by hydraulic pressure, and the loading value and rate were monitored by the force sensor in the jack. In the test, the specimens were loaded in stages (40 kN for each stage, holding for 5 min). The test could not be stopped until the specimens failed to bear the load or reached the upper limit of the load provided by the test equipment.

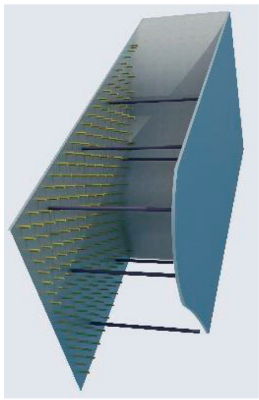

Internal structure diagram of typical components of nuclear power plant steel plate concrete shear wall

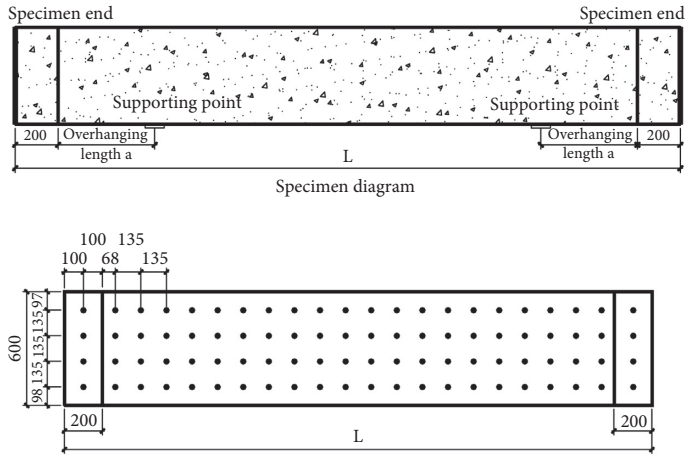

Figure 1: Diagrams of steel-concrete composite shear wall and specimens.

Table 1: List of specimen dimensions.

No.	Specimen no.	Width H/mm	Height T/mm	Total length L/mm	Test span/mm	Thickness of surface steel plate t/mm	Stud diameter d/mm	Stud length D/mm	Stud spacing B/mm	Concrete height–plate thickness ratio T/t	Shear span ratio	B/t
1	SC-P1	600	450	3100	1800	4.5	9	72	135	100	2	30
2	SC-P2	600	450	3100	1800	4.5	9	72	67.5	100	2	15
3	SC-P3	600	450	4900	2700	4.5	9	72	135	100	3	30
4	SC-P4	600	450	7200	4500	4.5	9	72	135	100	5	30
5	SC-P5	600	675	7200	4500	4.5	9	72	135	150	3.33	30

Table 2: Mechanical parameters of steel plate.

Material category	Test item	Test data
Steel plate (Q235B)	Yield strength/MPa	341
	Ultimate tensile strength/MPa	467
	Elastic modulus/MPa	$2.06e^5$
	Elongation	31.5%

Table 3: Mechanical parameters of concrete.

Material category	Test item	Test data
Concrete (C30)	Cube compressive strength/MPa	44.1
	Elastic modulus	$3.02e^4$

2.3. Instrumentation. The failure modes of steel plate-concrete wall slab specimens during the test were observed, and the failure process and crack distribution were recorded. The test data included the following: (1) vertical load exerted by the hydraulic jack on top of the loading beam (No. W4), (2) vertical displacements at the midspan and one-fourth span of the slab (No. W3), (3) vertical displacements at the supports (Nos. W1 and W2), (4) sliding condition between the surface steel plate and inner concrete (No. W1), and (5) strain of infill concrete under loading. Figure 3 shows the position of the measuring point of the displacement gauge (W1-W5).

Regarding concrete strain gauges, five gauges were arranged 10 mm away from the upper surface steel plate, along the beam length direction with the midline of the beam as the midpoint. Five gauges were arranged 10 mm away from the lower surface steel plate, along the beam length direction with the midline of the beam as the midpoint. Five gauges were also arranged at the midspan of the beam and placed close to the concrete strain gauges of the upper and lower surface steel plates, along the beam height. The arrangement at the one-fourth span was the same as that at the midspan of the beam. The strain rosettes were arranged in the inclined shoulder crack area at 0°, 45°, and 90°, as shown in Figure 4.

For steel plate strain gauges, five gauges were arranged symmetrically with the midline as the symmetrical axis on the beam surface (spacing at 100 mm), as shown in Figure 5.

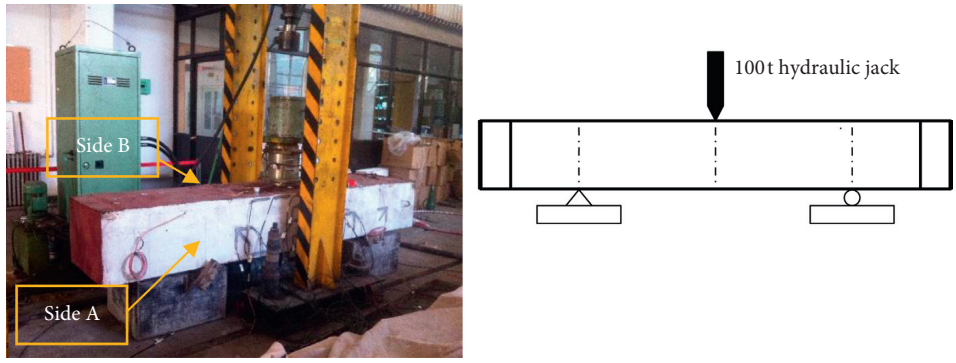

Figure 2: Loading equipment for specimens.

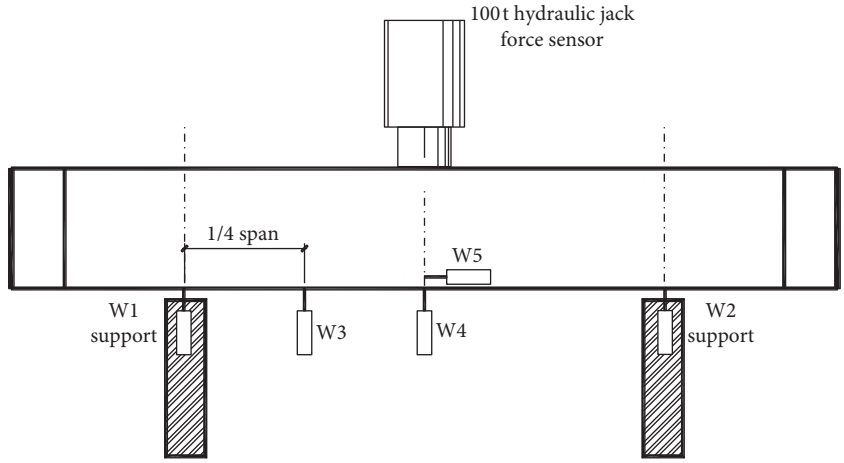

Figure 3: Displacement meter arrangement.

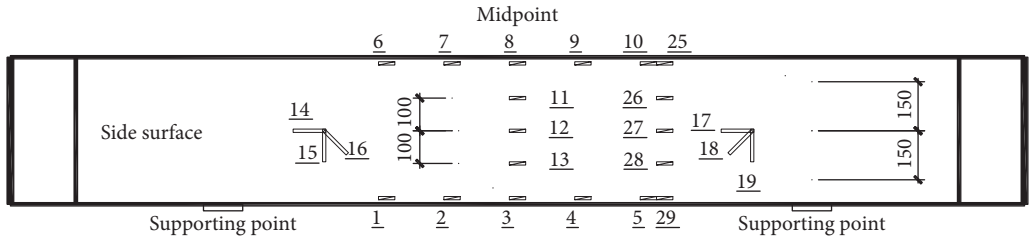

Figure 4: Arrangement of concrete strain gauges.

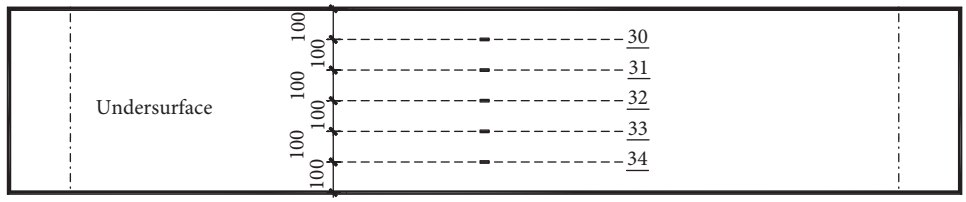

Figure 5: Arrangement of steel plate strain gauges.

3. Experimental Results and Analysis

3.1. Experimental Phenomena. No abnormal phenomenon was observed before the SC-P1 reached a peak load of 200 kN. At 200 kN, the specimen suffered a slender crack stretching from the bottom to the top. At 560 kN, a 0.2 mm wide vertical crack at the midspan existed on Side A of the specimen, as shown in Figure 6. At 640 kN, the crack

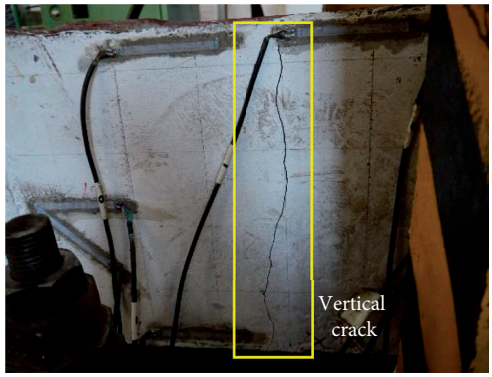

Figure 6: Vertical crack.

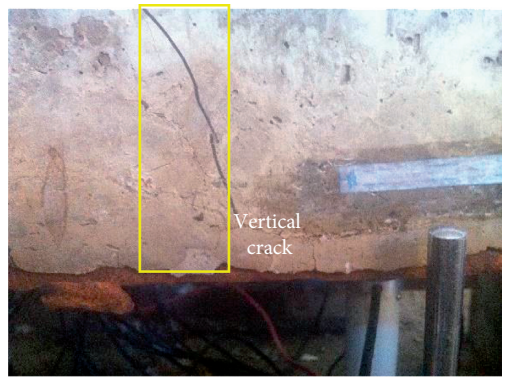

Figure 7: Vertical crack on side B.

occurred at the position of Side B corresponding to that of Side A (Figure 7). At 680 kN, the cracks continued to widen, but no new cracks appeared. At 800 kN, the cracks near the midspan bent toward the centerline, and those at the loading point began to stretch toward the centerline diagonally. At 840 kN, the concrete at 1/4 of Side B began to peel off. The specimen was finally loaded to the limit value of 999.94 kN.

SC-P2 had almost the same phenomena as SC-P1. However, the loads corresponding to the appearance of initial cracks on Sides A and B were different, that is, 240 and 520 kN, respectively. At 760 kN, the crack at the midspan was greater than 0.4 mm, and the concrete began to peel off slightly. Before the load reached a maximum of 998.04 kN, no new cracks appeared on the specimen, but the existing cracks widened continuously.

The crack occurred at the midspan of SC-P3 at 240 kN (Figure 8). With the increase in load, small cracks occurred near the initial one. At 600 kN, an evident gap was observed between the concrete in the midspan of the specimen and the steel plate, but it had a minimal change. At 700 kN, the steel plate yielded. The specimen was loaded continuously until it failed (Figure 9), corresponding to the ultimate load of 850 kN.

Before 120 kN, SC-P4 was in the elastic stage. At 134 kN, the concrete had a crack with a width of less than 0.1 mm. At 240 kN, the member had a slight sound, the stud was separated from the concrete, and a vertical crack appeared at the midspan. With the increase in load, the crack at the midspan continued to stretch upward. At 320 kN, Points 1 and 2 on the upper part had cracks and shrinkage strain. At 360 kN, a crack occurred outside the 1/4 span, and the cracks at the midspan continued to widen. At 440 kN, the steel plate yielded. At 480 kN, the specimen failed to bear the load.

At 200 kN, a crack was found in the internal concrete of SC-P5. At 240 kN, a crack occurred at the midspan. At 280 kN, the cracks stretched. With the increase in load, the cracks continued to widen, but no new cracks appeared. At 320 kN, the crack at the midspan continued to develop, and new cracks occurred at the one-fourth span and stretched rapidly toward three-fourths of the wall height. In addition, new cracks appeared on both sides of the wall. At 360 kN, the gap at the connection surface between the steel plate and concrete increased (Figure 10). At 400 kN, an inclined crack appeared at one-fourth span and developed toward the top

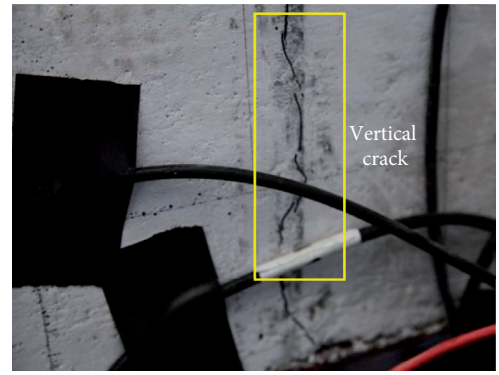

Figure 8: Vertical crack.

Figure 9: Specimen failure.

of the wall at 75° (Figures 11 and 12). As the load continued to increase, the steel plate and concrete slipped. The former yielded at 680 kN, and the latter was crushed at 733 kN.

Figures 13–17 show the crack distributions of SC-P1 to SC-P5, respectively.

3.2. Result Analysis. Table 4 shows the out-of-plane loading test results of steel plate-concrete slabs. In this table, P_{cr}, P_y, and P_u refer to the cracking, yielding, and ultimate loads, respectively. Δ_{cr}, Δ_y, and Δ_u refer to the midspan deflections corresponding to the cracking, yielding, and ultimate loads, respectively.

Figure 10: Cracks and gap at the connection surface.

Figure 11: Inclined crack.

Figure 12: Inclined crack.

3.2.1. Influence of Stud Spacing on Out-of-Plane Bending Shear Performance. Figure 18 shows the load-midspan deflection curves of SC-P1 and SC-P2. The longitudinal stud spacing of SC-P1 is twice that of SC-P2. The bending stiffness of SC-P2 is greater than that of SC-P1. The higher bending stiffness of SC-P2 is due to the smaller stud spacing of SC-P2 and the larger number of studs. The studs enhance the interfacial connection between the concrete part and the steel plate, which contributes to the larger stiffness of the specimen. Additionally, the studs can restrain the development of diagonal cracks, which is also beneficial.

Figures 19 and 20 show that the concrete near the bottom steel plate is in tension at the beginning of loading. Along the concrete cracking, the concrete on both sides of the crack reduces, turning the strain value at some positions into a negative value. According to the load-strain curve of the bottom steel plate, the tensile force in the middle of the bottom steel plate is evidently larger than that on both sides. With concrete cracking, the bottom steel plate bears more tensile force. The bottom steel plate of the SC-P1 and SC-P2 specimens does not enter into plasticity.

The comparison of the load-strain curves of concrete and the bottom steel plate for specimens SC-P1 and SC-P2 (Figure 19 to Figure 21) shows that, under the same load, the concrete strain value of SC-P1 is significantly higher than that of SC-P2, and the strain value of the bottom steel plate is significantly lower than that of SC-P2. When specimen SC-P1 reaches the ultimate load, the maximum strain of the bottom steel plate is 1,694.66 $\mu\varepsilon$, which is close to the yield value. Compared with the crack distribution of SC-P1, the crack development of SC-P2 is restrained due to the denser stud and the strong integrity of SC-P2. Transferring the load from the concrete to the steel plate is more efficient because the bottom steel plate bears more tension and thus yields earlier.

3.2.2. Influence of Shear Span Ratio on Out-of-Plane Bending Shear Performance. SC-P1, SC-P3, and SC-P4 have the same cross-section size, but their shear span ratios are 2, 3, and 5, respectively. Figure 22 shows that the initial stiffness values of SC-P1 and SC-P3 are nearly the same, but the stiffness of SC-P5 is evidently lower than those of the former two. With the increase of the shear span ratio, the failure mode of the member changes from diagonal compression to diagonal tension. The cracking load of SC-P3 is nearly the same as those of SC-P1 and SC-P2, but the load-strain curve of the bottom steel plate of SC-P3, as shown in Figure 23, indicates that the strain of the steel plate exceeds 2,000 microstrains when the load reaches approximately 700 kN, causing the bottom steel plate to yield. Diagonal tension brittle failure occurs when the specimen reaches the ultimate load.

3.2.3. Influence of Steel Contents on Out-of-Plane Bending Shear Performance. The shear span ratios of SC-P3 and SC-P5 are 3.00 and 3.33, respectively. The comparison of the load-strain curves of specimens SC-P3 and SC-P5 shows that an increase in the steel content can enhance the ultimate load-carrying capacity and ductility, as shown in Figure 24. Given the large height of the section of SC-P5, shear crack occurs directly. Once the concrete cracks, the crack width increases continuously. The steel plate will bear most of the tensile force until it yields. This phenomenon can also be seen from the comparison of the load-strain curve of the bottom steel plate, as shown in Figure 25.

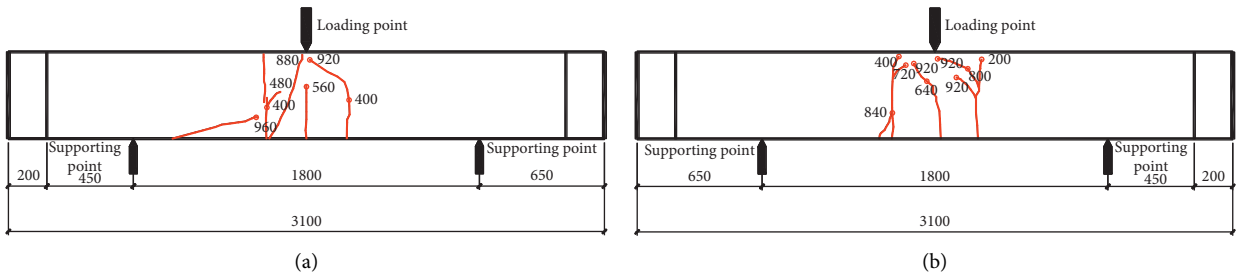

Figure 13: Crack distribution of SC-P1. (a) Crack distribution on Side A and (b) crack distribution on Side B.

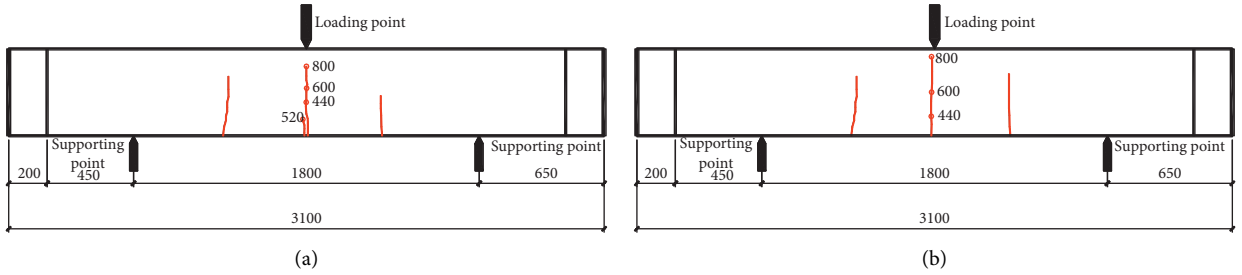

Figure 14: Crack distribution of SC-P2. (a) Crack distribution on Side A and (b) crack distribution on Side B.

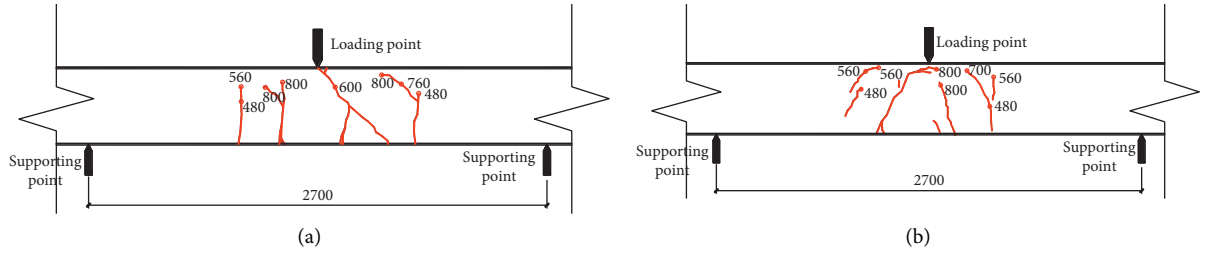

Figure 15: Crack distribution of SC-P3. (a) Crack distribution on Side A and (b) crack distribution on Side B.

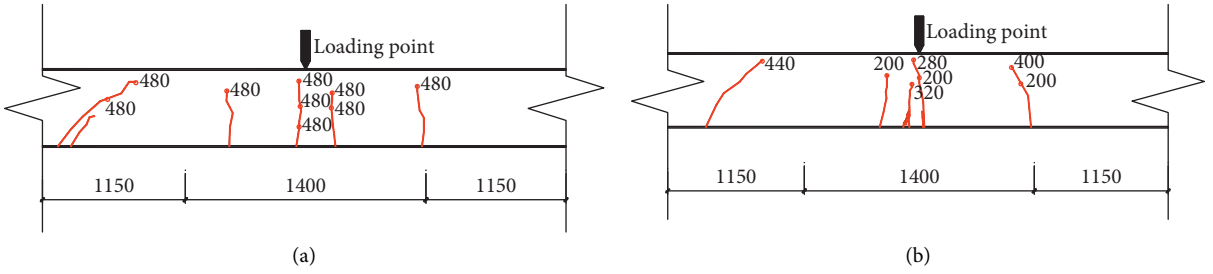

Figure 16: Crack distribution of SC-P4. (a) Crack distribution on Side A and (b) crack distribution on Side B.

4. Theoretical Analysis and Calculation

Three failure modes often occur to double-sided steel plate-concrete composite members: (1) bending, (2) horizontal sliding, and (3) vertical shear failures. Oblique shear failure occurs due to insufficient shear capacity of concrete or studs. After the abovementioned failure modes occur, buckling failure, which is determined by the spacing of the top shear connectors, may subsequently occur to the top steel plate when the loading is continued.

4.1. Bearing Capacity of Stud Connectors. On the basis of the actual conditions and failure modes of the specimens in this

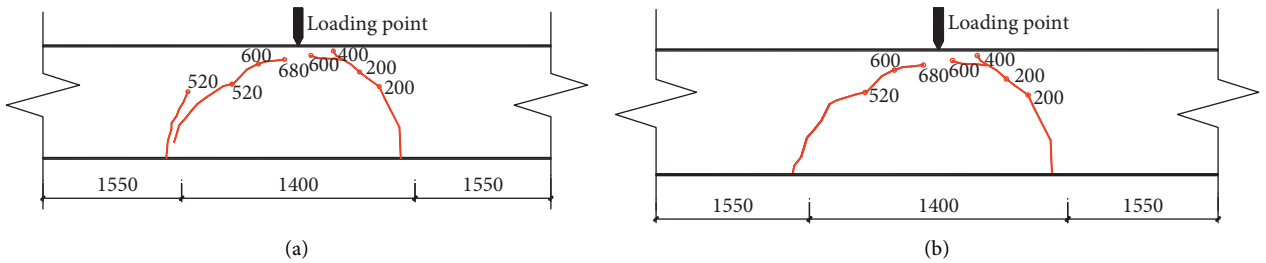

Figure 17: Crack distribution of SC-P5. (a) Crack distribution on Side A and (b) crack distribution on Side B.

Table 4: Main results of the out-of-plane loading tests on steel plate-concrete slabs.

Specimen no.	P_{cr}/kN	Δ_{cr}/mm	P_y/kN	Δ_y/mm	P_u/kN	Δ_u/mm
SC-P1	200	2.21	–	–	999.86*	9.87*
SC-P2	200	0.01	921.07	4.73	998.29*	5.39*
SC-P3	200	3.51	695.64	6.55	857.92	28.18
SC-P4	200	5.51	320.17	9.62	485.33	36.98
SC-P5	200	1.83	439.34	4.74	733.46	21.65

Note. *refers to the maximum load rather than the ultimate load.

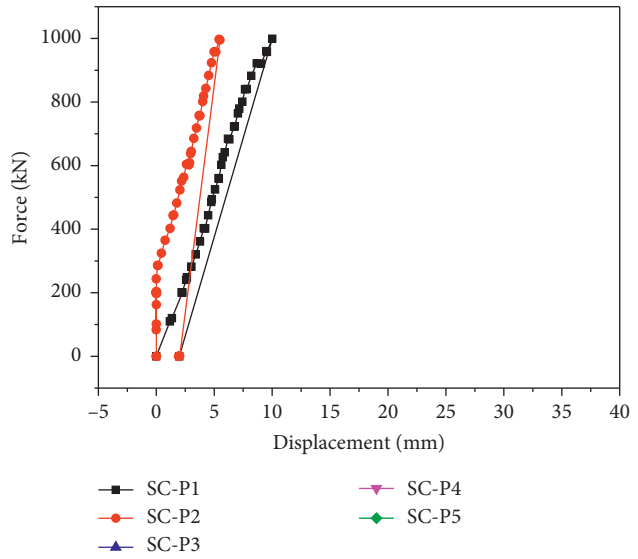

Figure 18: Load-midspan deflection curves of SC-P1 and SC-P2.

study and with reference to the research results of Roberts et al., the formulas for calculating the bearing capacity of double-sided steel plate-concrete members are as follows.

The shear capacity of stud connectors on the steel plates in tension and compression is as follows:

$$P_{cRd} = \frac{0.8P_{Rk}}{\gamma_v},$$
$$P_{tRd} = \frac{0.6P_{Rk}}{\gamma_v}, \quad (1)$$

where P_{cRd} is the shear capacity of stud connectors on the compression side of the steel plate, P_{tRd} is the shear capacity of stud connectors on the tension side of the steel plate, P_{Rk} is the shear capacity of a single stud, and γ_v is the safety factor of the stud material, $\gamma_v = 1.25$.

$$P_{Rk} = \min\left(\frac{0.8 f_u \pi d^2}{4}, 0.29\alpha d^2 \sqrt{f_{ck} E_{cm}}\right),$$
$$\alpha = 0.2\left(\frac{h_s}{d} + 1\right) \quad for 3 \le \frac{h_s}{d} \le 4, \quad (2)$$
$$\alpha = 1 \quad for \frac{h_s}{d} \ge 4,$$

where d and h_s are the diameter and height of the stud, respectively, f_u is the ultimate tensile strength of the stud,

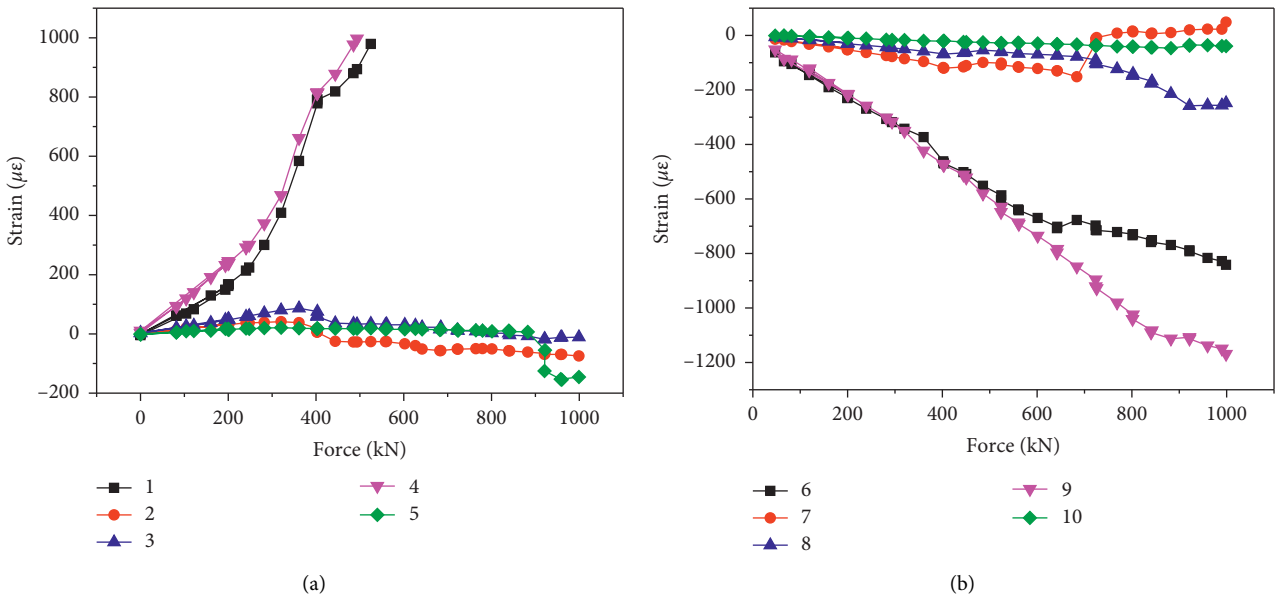

Figure 19: Load-strain curves of concrete fiber of SC-P1. (a) Lower fiber; (b) upper fiber.

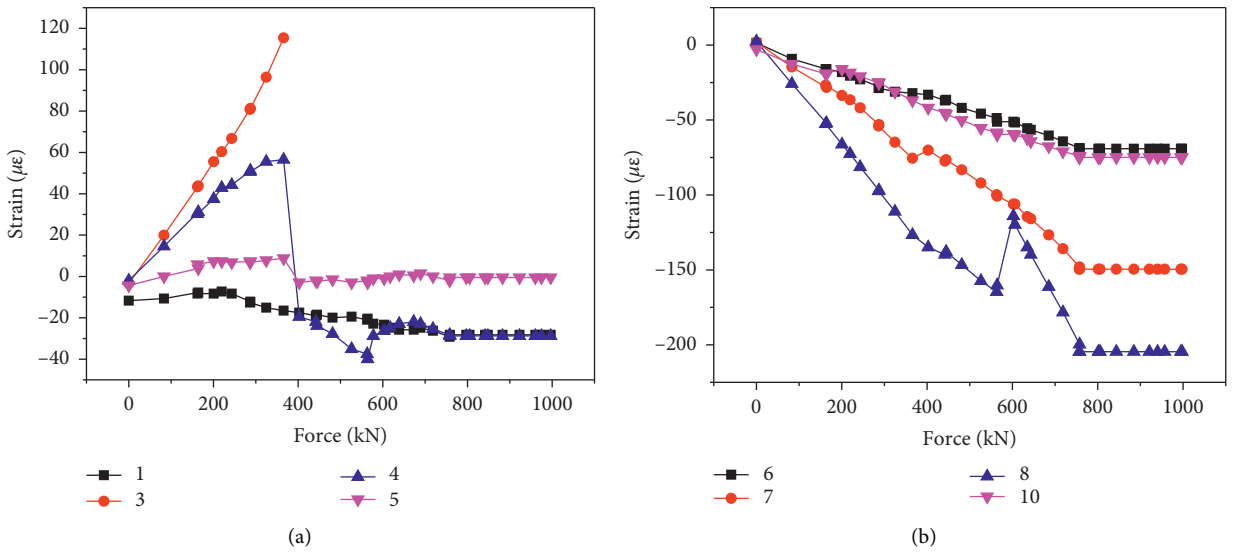

Figure 20: Load-strain curves of concrete fiber of SC-P2. (a) Lower fiber; (b) upper fiber.

f_{ck} is the axial compressive strength of concrete, and E_{cm} is the secant modulus of concrete.

4.2. Bending Capacity of Members. To calculate the ultimate bending capacity of the steel plate-concrete wall slabs, the stress diagram of the compression zone of the concrete was assumed to be rectangular, and the steel plate was subjected to axial force, as shown in Figure 26. The concrete below the neutral axis was assumed to crack, and the influence of its tensile strength was neglected.

The concrete pressure formula is as follows:

$$N_{cuRd} = 0.675 f_{cu} b \frac{0.9x}{\gamma_c}, \tag{3}$$

where f_{cu} is the cube compressive strength of concrete and γ_c is the safety factor of the concrete material: $\gamma_c = 1.5$.

The forces of the steel plate in compression and tension were mainly determined by the yield of the steel plate or the sliding yield of the stud, as shown in the following formulas:

$$\begin{aligned} N_{cuRd} &\le \frac{A_{sc} f_{sc}}{\gamma_\alpha} \le n_c P_{cRd}, \\ N_{tRd} &\le \frac{A_{st} f_{yst}}{\gamma_\alpha} \le n_t P_{tRd}, \end{aligned} \tag{4}$$

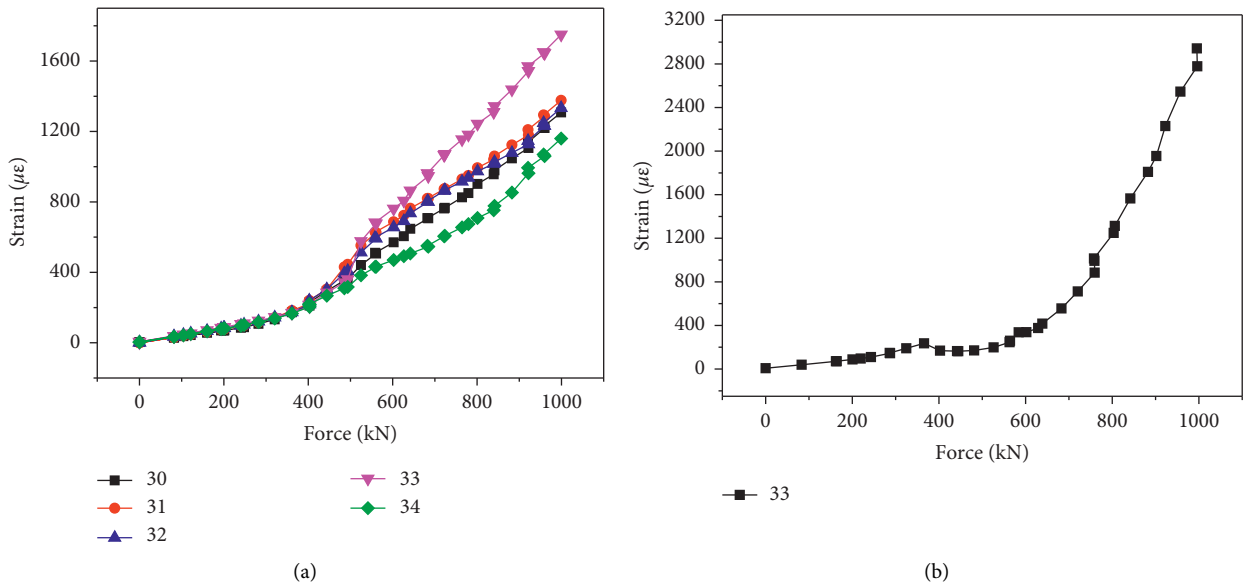

Figure 21: Load-strain curves of bottom steel plates of (a) SC-P1 and (b) SC-P2.

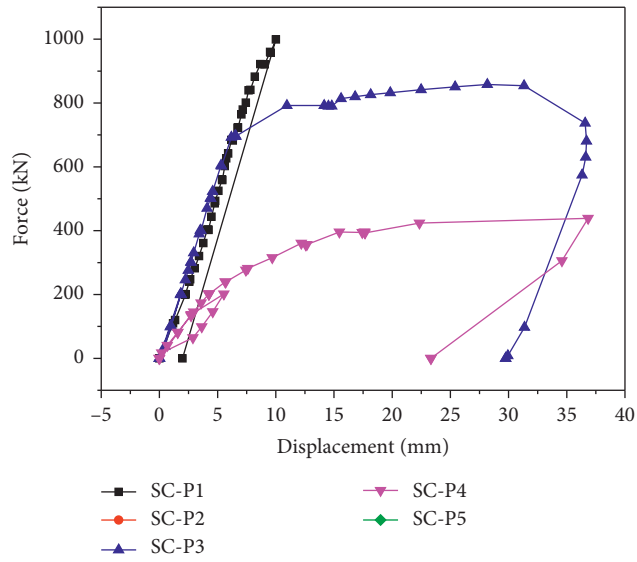

Figure 22: Load-midspan deflection curves of SC-P1, SC-P3, and SC-P4.

where A_{sc} and A_{st} are the cross-sectional areas of the steel plate on the compression and tension sides, respectively; f_{sc} and f_{yst} are the uniaxial yield strengths of the steel plate on the sides in compression and tension, respectively; and n_c and n_t are the numbers of effective stud connectors on the compression and tension sides, respectively.

The height formula of the plastic neutral axis is as follows:

$$x = \frac{(N_{tRd} - N_{cRd})\gamma_c}{0.6075 f_{cu} b}. \quad (5)$$

The ultimate bending capacity is as follows:

$$M_{Rd} = N_{tRd}\left(h_c + \frac{t_{sc}}{2} + \frac{t_{st}}{2}\right) - N_{cuRd}\left(0.45x + \frac{t_{sc}}{2}\right). \quad (6)$$

4.3. Shear Capacity of Members. For steel plate-concrete members, the surface steel plate has minimal contribution to the shear capacity, which can be neglected. Thus, the ultimate shear capacity can be contributed by concrete and studs. Considering that the full-section shear of the concrete and the shear resistance of the stud connectors would not occur simultaneously, the factor was set to 0.5, and the effect of the studs was reduced:

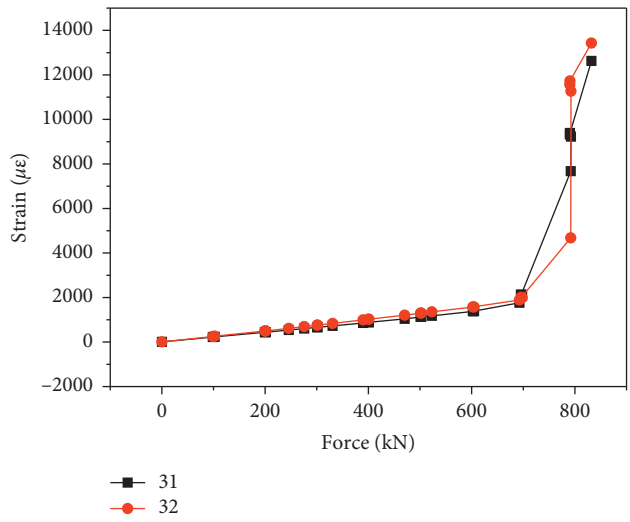

Figure 23: Load-strain curves of bottom steel plates of SC-P3.

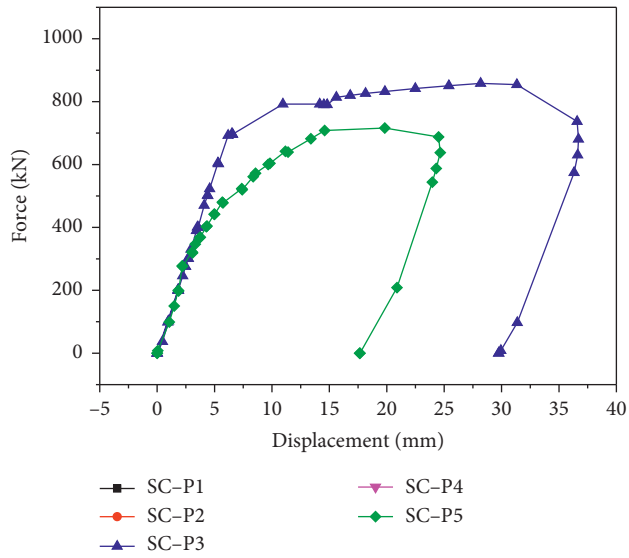

Figure 24: Load-midspan deflection curves of SC-P3 and SC-P5.

$$V_{Rd} = \tau_{Rd} b h_c,$$
$$\tau_{Rd} = \frac{f_{ck}}{20\gamma_c} + \frac{0.5 n_0 A_s f_u}{b s_t \gamma_a}, \quad (7)$$

where A_s and f_u are the cross-sectional area and ultimate tensile strength of the stud, respectively, and n_0 is the number of studs in the cross-sectional direction.

4.4. Comparison between Theoretical Calculation and Test Results. The previous formula was used to calculate the actual conditions and failure modes of the specimens, and the calculation results were compared with the test results, as shown in Tables 5 and 6. The results showed that the test values were higher than the theoretical ones. Therefore, the results were safe with the theoretical formula for designing and calculating the steel sheet concrete members.

P_u is the ultimate load of the specimens in the test, where SC-P1 and SC-P2 were undamaged; thus, no comparison was made between them. V_c is the shear capacity of the member calculated using the formula. V_{test} is the shear value corresponding to the load when the specimen has shear failure. V_{test}/V_c is the ratio of the test and calculated values.

5. Numerical Simulation

5.1. Model Comparison. The simulation calculation and analysis were conducted using ANSYS general finite element calculation software. Initially, the simulation results were compared with the test results through finite element analysis to verify the correctness of the calculation model. On this

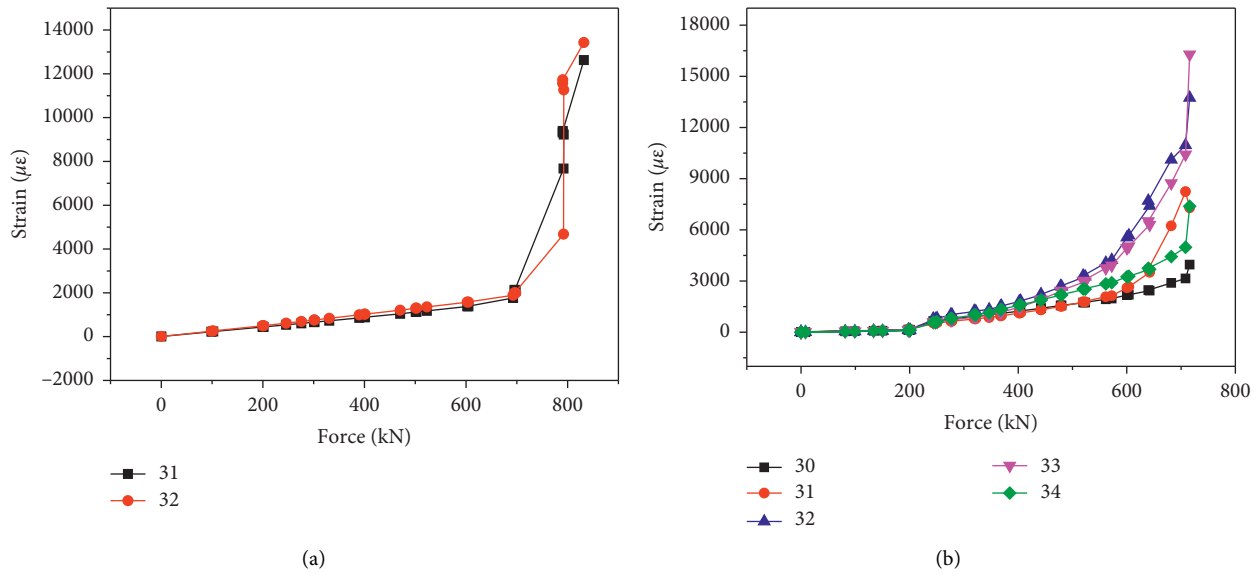

Figure 25: Load-strain curves of bottom steel plates of (a) SC-P3 and (b) SC-P5.

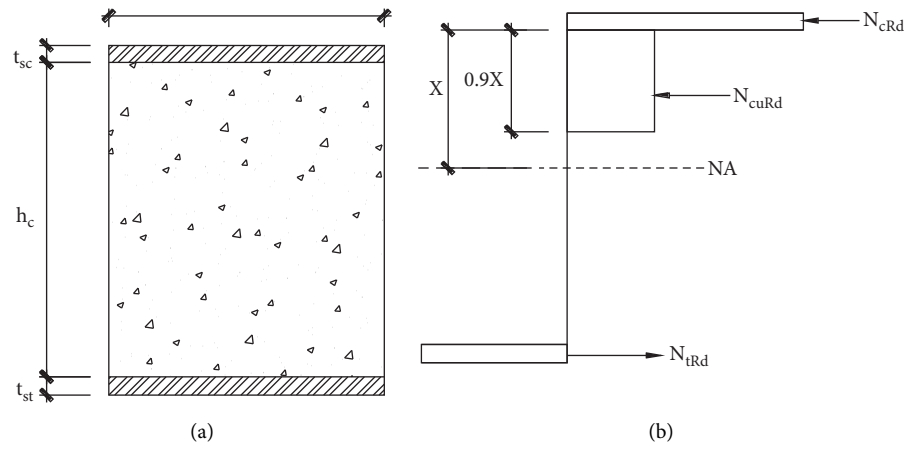

Figure 26: Theoretical calculation diagram.

Table 5: Comparison between the test and theoretical results of the out-of-plane shear capacity of steel plate-concrete slabs.

No.	P_u/kN	P_c/kN	$\frac{P_u}{P_c}$	V_{test}/kN	V_c/kN	$\frac{V_{test}}{V_c}$	Failure mode
SC-P1	999.86	–	–	–	–	–	Shear failure
SC-P2	998.29	–	–	–	–	–	Shear failure
SC-P3	857.92	581.63	1.47	**428.62**	**229.81**	**1.87**	Shear failure

Table 6: Comparison between the test and theoretical results of the out-of-plane bending capacity of steel plate-concrete slabs.

No.	P_u/kN	P_c/kN	$\frac{P_u}{P_c}$	V_{test}/kN	V_c/kN	$\frac{V_{test}}{V_c}$	Failure mode
SC-P4	**485.33**	**348.98**	**1.39**	242.67	229.81	1.06	Bending
SC-P5	**733.46**	**533.12**	**1.38**	366.73	229.81	1.56	Bending

basis, the influences of steel plate thickness and stud spacing on the bending-shear behaviors of the steel plate-concrete structure were further studied via parametric analysis.

A 3D solid numerical model was established on the basis of the actual sizes and material parameters of the specimens. The concrete member was modeled with element Solid65. The stress-strain curve of concrete is determined in accordance with the Code for Design of Concrete Structures (GB 50010–2010). The Poisson ratio is 0.173. The steel plate was modeled with element Shell181. The stress strain of the steel plate is elastic-perfectly plastic. The elasticity modulus of steel is 2.0×10^5 MPa, and the Poisson ratio is 0.3. The joints between the concrete and steel members were modeled with

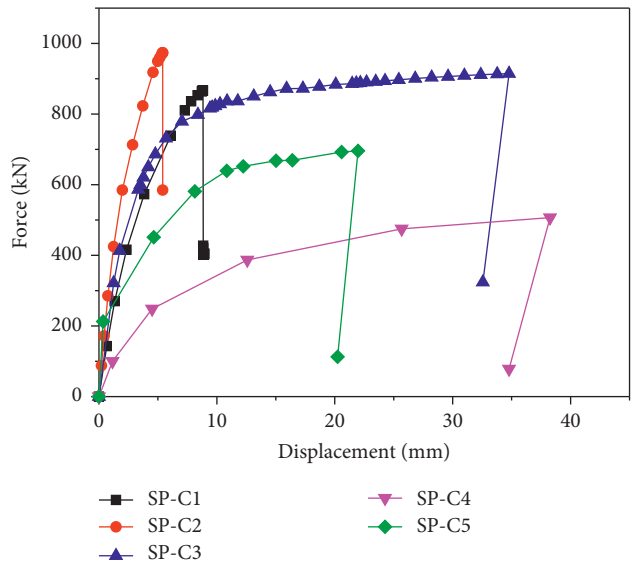

Figure 27: Load-deformation curves of all members.

the Combine39 element in the X, Y, and Z directions. The Combine39 element was distributed on the basis of the locations of the stud connectors.

The simulation models were loaded with three-point bending. Figure 27 depicts the simulation results of the load-deformation curves for the members. The ultimate load was compared with the experimental results, as shown in Table 7. The comparison shows that the calculated results are near the experimental results. Therefore, the calculation model could be adopted to predict the failure mode and stress process of the steel plate-concrete structure specimens.

Table 7: Comparison between the test result and the simulation results.

Member	P_u/kN		Δ_u/mm	
	Test	Simulation	Test	Simulation
SC-P1	999.86*	864.25	9.87*	9.98
SC-P2	998.29*	976.55	5.39*	5.25
SC-P3	857.92	900.23	28.18	29.01
SC-P4	485.33	500.65	36.98	37.20
SC-P5	733.46	677.46	21.65	22.06

5.2. Parametric Analysis

5.2.1. Steel Plate Thickness. The steel plate thickness was set to 4.5, 6.5, 8.5, 10.5, and 12.5 mm to investigate its influence. The dimension and material parameters of members were the same as those of SC-P1. The simulation unit was similar to the one mentioned above. The material properties are identical to one another. The simulation models were loaded with three-point bending. Figure 28 depicts the stress distributions of the steel plate, and Figure 29 shows the mid-span load-displacement curves of the members.

When the steel plate was 4.5–10.5 mm thick, the ultimate bearing capacity of the members increased with the thickness. However, when the steel plate was 12.5 mm thick, the stiffness of the members and the ultimate bearing capacity were reduced, affected by the debonding of the steel plate-concrete interface.

When the steel plate thickness was less than 10.5 mm, with the increase in thickness, the overall stress distribution of the steel plate tended to be uniform. In addition, the mutual deformation between the steel plate and concrete component was in harmony, thereby fully playing the role of materials. Therefore, with the increase in steel plate thickness, the ultimate bearing capacity of members continued to increase.

When the steel plate thickness reached 12.5 mm, the ultimate bearing capacity of the member was lower than that of the specimen with the 10.5 mm thick steel plate, which was due to the debonding of the steel plate-concrete interface. When the steel plate stiffness was high, the bending stiffness of steel plate and concrete component varied significantly. With the increase in member deformation, the normal and shear stresses at the interface between the steel plate and concrete component increased. When they exceeded the resistance of the studs, the interface would begin to slide, thereby decreasing the ultimate bearing capacity of members.

5.2.2. Stud Spacing. To study the influence of stud spacing on the out-of-plane shear-bending behavior of steel plate-concrete wall slabs, a finite element model was established to calculate the stud spacing of 67.5, 135, 270, and 405 mm. Other dimensions and material parameters of the model were the same as those of SC-P1. The simulation models were loaded with three-point bending. Figure 30 shows the stress distributions of the steel plate, and Figure 31 shows the load-deformation curves of the members with different stud spacings.

When the stud spacing was 270 mm, the member suffered interface debonding, reduced stiffness, and decreased

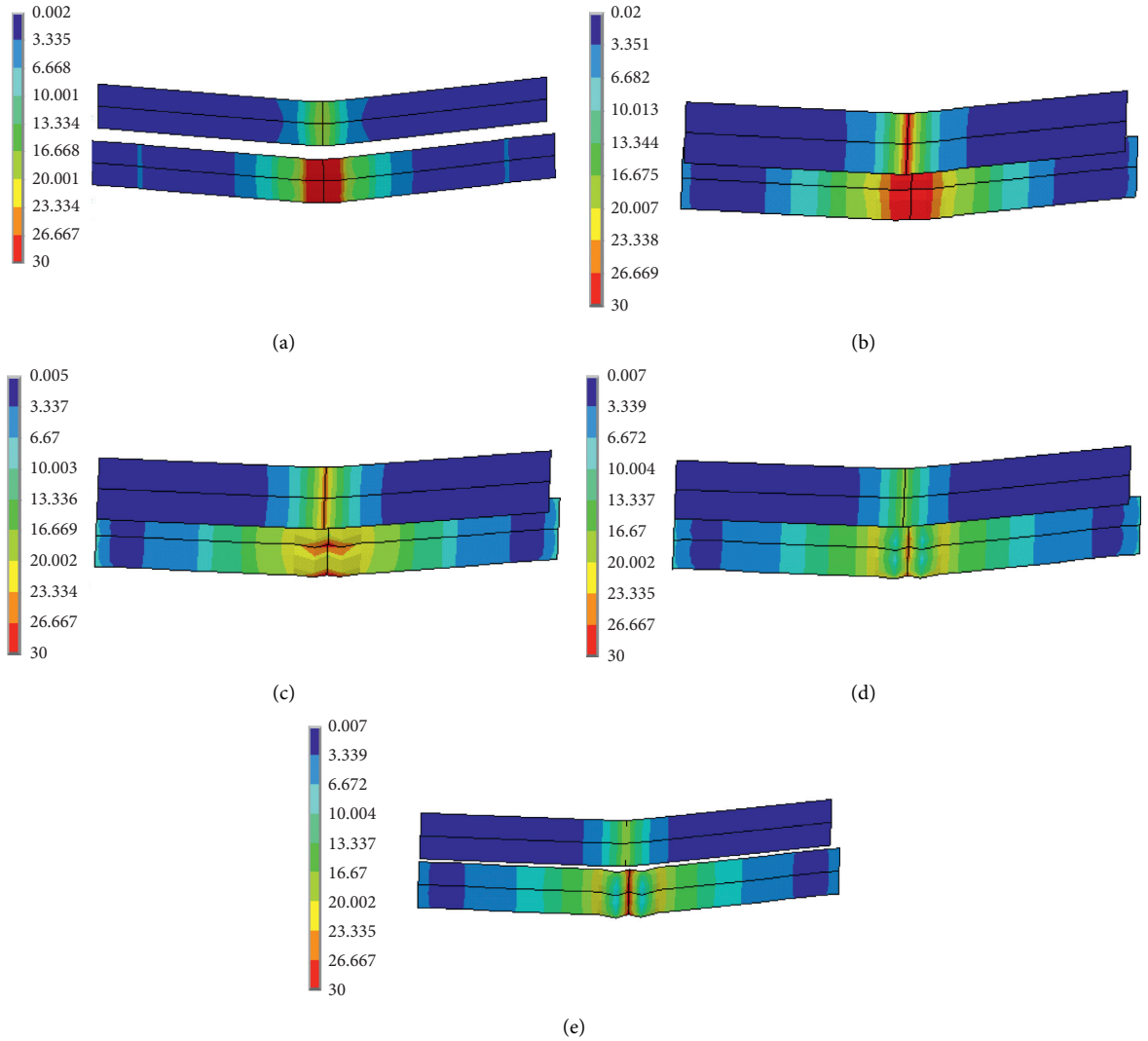

Figure 28: The stress distribution of steel plates when the thickness is changed. (a) The thickness of steel plate is 4.5 mm. (b) The thickness of steel plate is 6.5 mm. (c) The thickness of steel plate is 8.5 mm. (d) The thickness of steel plate is 10.5 mm. (e) The thickness of steel plate is 12.5 mm.

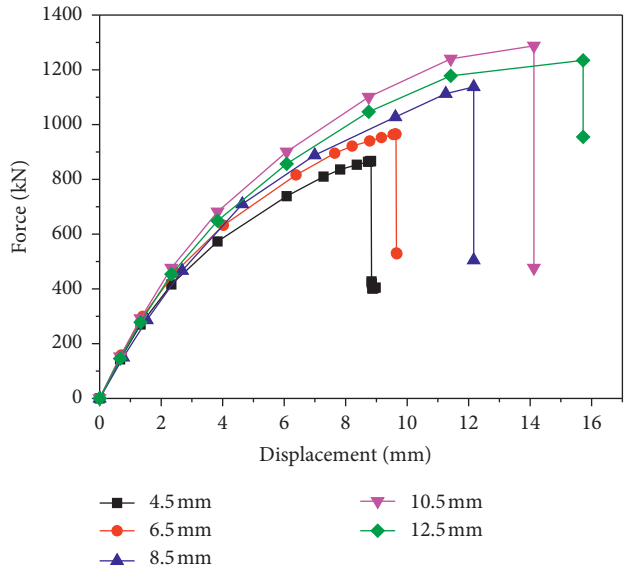

Figure 29: Load-displacement curves of all models.

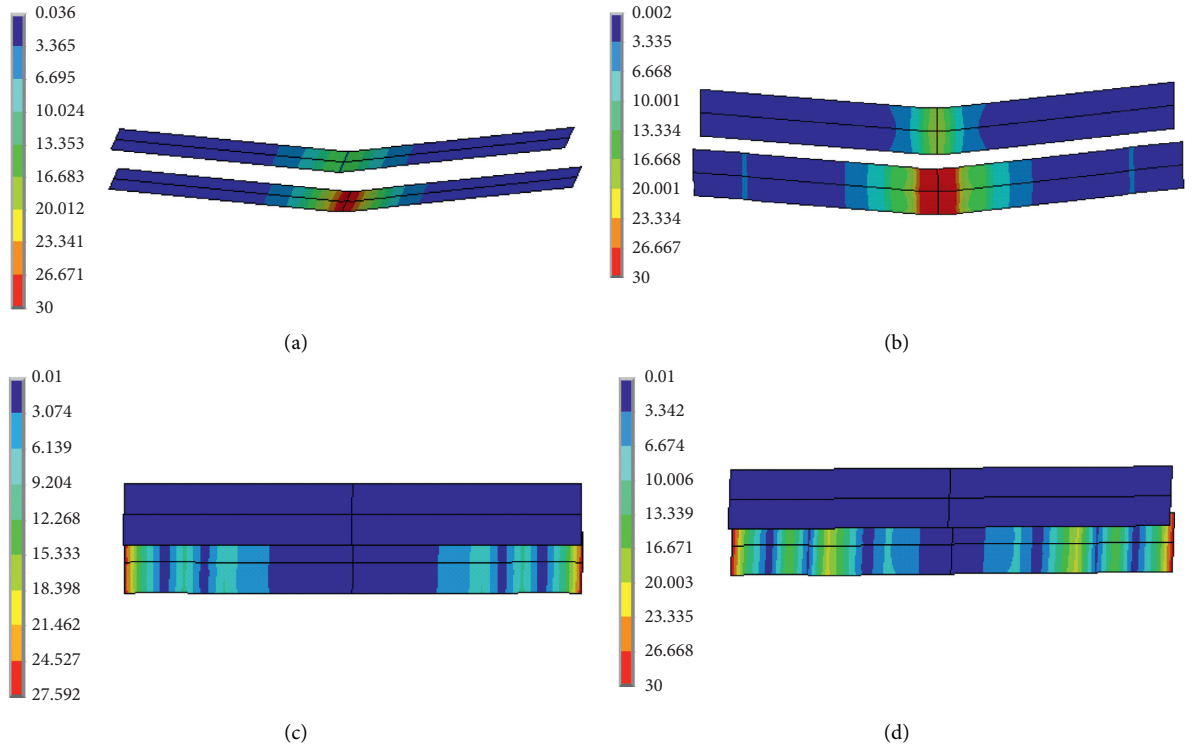

Figure 30: The stress distribution of steel plates when the stud spacing is changed. (a) Stud spacing of 67.5 mm. (b) Stud spacing of 135 mm. (c) Stud spacing of 270 mm. (d) Stud spacing of 405 mm.

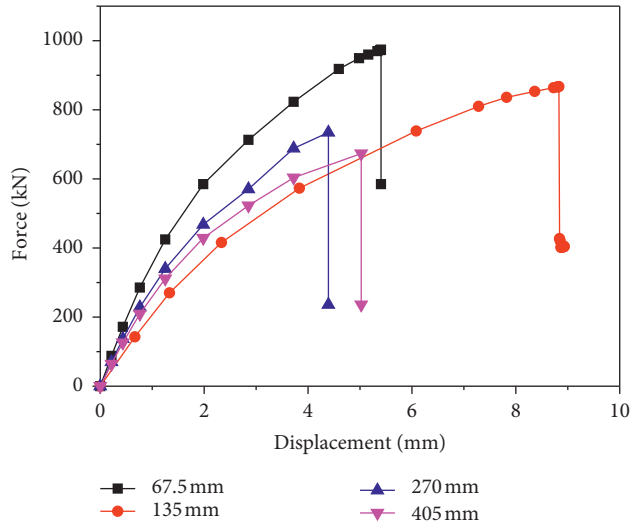

Figure 31: Load-displacement curves of members with different stud spacing.

ultimate bearing capacity. When the stud spacing was 405 mm, the studs were insufficient, leading to the interface debonding of the steel plate and the further decrease of the ultimate bearing capacity of the member.

6. Conclusions

In this study, test and finite element analysis were conducted on five steel plate-concrete wall slab specimens with different stud spacings, shear span ratios, and steel contents. The following conclusions were drawn:

(1) The steel plate-concrete wall slab under the out-of-plane load had the same failure mode as that of an ordinary reinforced concrete wall. This case was mainly the brittle failure without setting the shear key.

(2) In the case of numerous studs, the out-of-plane shear capacity of the steel plate-concrete wall slab increased significantly.

(3) With the increase in shear span ratio, steel plate-concrete members suffered a bending failure.

(4) When the steel content was low, the steel plate-concrete wall slab directly had a shear failure.

(5) With the increase in steel plate thickness, the ultimate bearing capacity of members also increased. However, when the steel plate was 10.5 mm thick, the ultimate load of members did not increase, and the steel plate did not yield. With the increase in stud spacing, the turning point of the deflection-stud sliding curve was advanced, the displacement amount of the stud increased, and the stiffness of the member decreased. When the stud spacing reached 400 mm, the member had steel plate debonding due to the insufficient quantity of studs.

(6) The formula to calculate the shear capacity of steel plate-concrete wall slabs was derived. In addition, the calculated margin was small when the shear span ratio of the member was extremely large.

Data Availability

The data used to support the findings of this study are available from the corresponding author upon request.

Conflicts of Interest

The authors declare that they have no conflicts of interest.

References

[1] Translation of J. E. A. G.. Technical Guidelines for Aseismic Design of Steel Plate Reinforced Concrete Structures Buildings and Structures.2005.

[2] ACI349, *Code Requirements for Nuclear Safety-Related Structural and Commentary*, American Concrete Institute, Farmington Hills, MI, USA, 2006.

[3] M. Takeuchi, *Experimental Study on Steel Plate Reinforced Concrete Structure Part 28 Response of SC Members Subjected to Out-Of-Plane Load 1*, pp. 1237-1238, Architectural Institute of Japan, Kanto, Japan, 1999.

[4] O. Tetsuya, "Experimental study on A concrete filled steel structure Part5 shear tests (discussion of parameters)," *Synopsis of Academic Lectures*, pp. 955-956, Architectural Institute of Japan, Kanto, Japan, 2006.

[5] T. O. S. Oduyemi and H. D. Wright, "An experimental investigation into the behaviour of double-skin sandwich beams," *Journal of Constructional Steel Research*, vol. 14, no. 3, pp. 197–220, 1989.

[6] T. Honda, *Experimental Study on Steel Plate Reinforced Concrete Structure Part 29 Response of SC Members Subjected to Out-Of-Plane Load 2*, pp. 1239-1240, Architectural Institute of Japan, Kanto, Japan, 1999.

[7] K. Ikeda, *Experimental Study on A Concrete Filled Steel Structrue Part. 3 Compressive Tests. Synopsis of Academic Lectures*, pp. 1241-1242, Architectural Institute of Japan, Kanto, Japan, 1999.

[8] S. Ryoichi, *Experimental Study on Steel Plate Reinforced Concrete Structure Part 31 Response of SC Members Subjected to Out-Of-Plane Load 4*, pp. 1243-1244, Architectural Institute of Japan, Kanto, Japan, 1999.

[9] S. G Hong, W. Kim, K. J. Lee, N. K. Hong, and D. H. Lee, "Out-of-plane shear strength of steel plate concrete walls dependent on bond behavior," in *Proceedings of 20th International Conference on Structural Mechanics in Reactor Technology*, Espoo. Finland, August 9–14 2009.

[10] H. Amit, *Out-Of-Plane Shear Behavior Of Sc Composite Structure*, 2011.

[11] Z. Liu and Z. Cao, "Dynamic analysis of steel-concrete composite plate structure," *Journal of Building Structures*, vol. 4, pp. 30–44, 1984.

[12] NieJieguo and J. Zhao, "Experimental study on simply supported steel plate-concrete composite plates," *China Civil Engineering Journal*, vol. 41, no. 12, pp. 28–34, 2008.

[13] J. Zhao and J. Nie, "Nonlinear finite element analysis of steel-concrete composite beams," *Engineering Mechanics*, vol. 26, no. 4, pp. 105–112, 2009.

[14] Y. Fang, Y. Sun, K. Qian, R. Pan, and C. Tian, "Experimental study of the out-of-plane seismic behavior of steel-concrete-steel sandwich composite shear wall," *Industrial Construction*, vol. 32, no. 11, pp. 22–29, 2011.

[15] Y. Leng, X. Song, H. Ge, and M. Chu, "Experimental study on out-of-plane shear resistance of steel-concrete composite wall structures," *Journal of Building Structures*, vol. 43, no. 22, pp. 15–21, 2013.

[16] M. Chu, X. Song, and H. Ge, "Structural performance of steel–concrete–steel sandwich composite beams with channel steel connectors," in *Proceedings of 22nd International Conferenceon Structural Mechanicsin Reactor Technology(SMiRT-22)*, San Francisco, USA, August 18–23, 2013.

[17] Y.-B. Leng and X.-B. Song, "Flexural and shear performance of steel-concrete-steel sandwich slabs under concentrate loads," *Journal of Constructional Steel Research*, vol. 134, pp. 38–52, 2017.

[18] Y. Yang and J. Liu, "Experimental study on flexural capacity of steel plate-concrete composite slabs," *Journal of Building Structures*, vol. 34, no. 1, 2013.

[19] X. Ji, X. Jia, and J. Qian, "Experimental study on shear behavior of steel-plate composite shear walls," *Journal of Building Structures*, vol. 36, no. 11, pp. 46–55, 2015.

[20] C. Chao and X. Song, "Research on steel-concrete unit biaxial repeated loading model," *Low Temperature Architecture Technology*, vol. 39, no. 4, pp. 15–19, 2017.